Journal of Power Sources 208 (2012) 316–321

Contents lists available at SciVerse ScienceDirect

Journal of Power Sources

journal homepage: www.elsevier.com/locate/jpowsour

Anatase TiO_2 beads having ultra-fast electron diffusion rates for use in low temperature flexible dye-sensitized solar cells

Chun-Ren Ke, Jyh-Ming Ting*

Department of Materials Science and Engineering, National Cheng Kung University, Tainan 70101, Taiwan

ARTICLE INFO

Article history:
Received 19 December 2011
Received in revised form 30 January 2012
Accepted 15 February 2012
Available online 23 February 2012

Keywords:
Mesoporous TiO_2 beads
Plastic substrate
Flexible dye-sensitized solar cell
Electron diffusion

ABSTRACT

The first use of mesoporous TiO_2 beads in plastic substrate flexible dye-sensitized solar cell (FDSC) is demonstrated. Pure anatase TiO_2 beads with various sizes (250–750 nm) and characteristics are obtained using a modified and efficient two-step method. The concept of chemical sintering, eliminating the step of additive removal, is used to prepare bead-containing paste for room temperature fabrication of photoanode having good adhesion to the substrate. The obtained photoanodes are examined for their dye loadings and light absorbance properties. Various plastic substrate FDSCs having commercial P25- and bead-containing photoanodes are fabricated and evaluated. The resulting cells are evaluated for the *J–V* characteristics, electron diffusion time, electron lifetime, charge-collection efficiency, electron-injection efficiency and incident photon-to-electron conversion efficiency. The bead-only cells not only have better efficiencies, as high as ~5%, but also exhibit ultra-fast electron diffusion rates, less than 1 ms (~0.37 ms, 7.6 μm). The best efficiency and electron diffusion rates are respectively 15% higher and two-order of magnitude faster than the P25-only cell. The effects of the bead characteristics on the cell performance is presented and discussed.

© 2012 Elsevier B.V. All rights reserved.

1. Introduction

Flexible dye-sensitized solar cell (FDSC) is a superior candidate for mobile electric power [1]. Especially, FDSCs having plastic substrates suitable for roll-to-roll production in large scale and doubled-faced illumination attract much attention. However, the required low photoanode synthesis temperatures severely limit charge-collection efficiency (η_{cc}) [2]. In order to resolve this problem, many approaches such as photoelectrode transfer [2], chemical sintering [3], and compression method [4] have been investigated. Other than developing various preparation technologies, novel TiO_2 photoanode structures, such as the use of nanotubes to replace nanoparticles, have also been investigated [5]. In general, photoanodes having TiO_2 nanoparticles suffer from electron loss during the electron transport through the randomly distributed 3-D network [6]. The use of oriented nanotube arrays have been shown to exhibit a faster electron diffusion time (τ_d) by allowing the electron transport in the direction of the tube axis [7]. Basically, the η_{cc} can be enhanced by reducing τ_d [8]. However, the nanotube-based photoelectrodes also exhibit an undesired porous structure and thereby give poor cell performance [9]. As a result, a particular TiO_2 structure called beads, exhibiting fast electron diffusion and excellent light-harvesting ability, have been recently introduced [10,11]. The submicron-size beads were used in the whole photoanodes [10–13] or scattering layers [14]. In both cases, the photoanodes were prepared at ~450 °C for use in rigid DSCs (RDSCs). In other words, so far, there is no report showing the use of such beads in plastic substrate FDSCs. Although the high-temperature synthesis of bead-containing photoanodes has been demonstrated, the fabrication of low-temperature version of bead-containing photoanodes is not straightforward.

In general, the pastes used in the conventional RDSCs contain uniformly and well dispersed TiO_2 due to the addition of binders such as poly-ethylene-glycol. However, such binders are difficult to be removed at room or low temperatures, e.g., 140 °C. In other words, the selection of a binder and other additives is severely limited, and binder-free pastes are desired. This is particularly true for the submicron-size TiO_2 beads, which sediment much faster than TiO_2 nanoparticles, such as commercial P25, as shown later. Another challenge is the adhesion between the low-temperature synthesized bead-containing photoanode and the plastic substrate. Pretreatment of glass substrate using $TiCl_4$ represents a common practice during the fabrication of RDCS for enhancing the adhesion [15]. However, such approach is not viable for plastic substrate FDSCs due to the vulnerable chemical resistance of the plastic to $TiCl_4$. As a result, in this paper, we use the concept of chemical sintering for the preparation of bead-containing paste [16]. Such an approach effectively resolves both the additive and adhesion issues. In our approach, $HCl_{(aq)}$ dissolving in absolute ethanol is used as the sole solvent for making the paste. The use of $HCl_{(aq)}$

* Corresponding author. Tel.: +886 6 238 5613; fax: +886 6 238 5613.
E-mail address: jting@mail.ncku.edu.tw (J.-M. Ting).

0378-7753/$ – see front matter © 2012 Elsevier B.V. All rights reserved.
doi:10.1016/j.jpowsour.2012.02.056

Table 1
Grain sizes, bead sizes, surface Ti^{4+} concentration of TiO_2 beads or nanoparticles (NPs) obtained at various conditions. For comparison, P25 is included.

Sample ID	Hexamine amount (g)	Hydrothermal temperature (°C)	Grain size (nm)	Bead size (nm)	BET surface area ($m^2\ g^{-1}$)	Total pore volume ($cm^3\ g^{-1}$)	Ti^{4+} concentration (%)
P25	–	–	22	–	54	0.13	55
A	0.75	120	14	375	95	0.27	65
B	0.75	160	18	750	69	0.27	91
C	0.75	200	20	500	62	0.25	93
D	0.50	200	20	250	62	0.27	93
E	0.25	200	20	NPs	63	0.26	93

protonizes the TiO_2 surfaces, giving improved viscosity and dispersion of the beads. Furthermore, a more efficient way of making TiO_2 beads is presented. The original synthesis utilizes hexadecylamine as the structure-directing agent [10]. In this study, hexamine, which is more soluble in water and therefore can be easily washed out by water, is used as the steric agent. Therefore, an added advantage is that the calcination step [10] is waived. Moreover, hexamine with tertiary amine structure is more effective steric agent, a small amount of which allows direct control of the sizes of the resulting beads. Using the obtained beads and the aforementioned paste preparation method, photoanodes were prepared using a compression technique, which is a room temperature process and results in satisfactory adhesion between the photoanode and the substrate. High efficiency FDSCs having bead-containing photoanodes are demonstrated and evaluated.

2. Experimental

TiO_2 beads were prepared using a sol–gel method followed by a hydrothermal process. The sol–gel solution consisted of x g (x = 0.25–0.75) of hexamine in 200 mL ethanol. The hexamine severed as the steric agent. 1 mL of KCl (0.1 M) was mixed into the sol–gel solution to change the ion strength in the reaction medium to control the size distribution of sol–gel products [17]. 4.4 mL of titanium (IV) isopropoxide (TTIP) was then poured into the mixture, allowing to the precipitation of particles. The obtained particles were mixed with de-ionized (DI) water and the resulting suspension fluid was loaded into an autoclave for hydrothermal treatment at various temperatures of 120, 160, and 200 °C for 6 hours. Paste consisting of the hydrothermally synthesized TiO_2 beads and commercial P25 TiO_2 powders was made by mixing the all TiO_2 powders in ethanol and HCl. The addition of HCl protonizes the TiO_2 surface, preventing the aggregation and then the sedimentation of the beads. For the fabrication of photoanode, the paste was first spun onto indium tin oxide (ITO)-coated polyethylene naphthalate (PEN) substrate, which was then dried in air for 10 min. This cycle repeated for two or three times to obtained the desired thickness. The active area of a photoanode was 4 mm × 4 mm. The multiple-layer coatings were then subjected to mechanical compression without any heat treatment for the formation of photoanodes. The thicknesses of the photoanodes were controlled to be 7.5–8.0 μm. Photoanode was immersed in an ethanol solution of commercial N719 dye (5×10^{-4} M) overnight for dye loading. FDSCs were assembled using an electrolyte consisting of 0.1 M LiI, 0.05 M I_2, 0.6 M 1,2-dimethyl-3-propylimidazolium iodide (DMPII), and 0.5 M 4-*tert*-butylpyridine (TBP) in 3-methoxypropionitrile (MPN) system and Pt-coated ITO-PEN as the counter electrode.

Various methods were used to characterize the photoanodes and the cells. The crystalline phases of TiO_2 photoanodes were identified using X-ray diffraction (XRD) and high-resolution transmission electron microscopy (HRTEM). The morphology of photoanodes was examined using scanning electron microscope (SEM). The surface chemistry of TiO_2 photoanode was examined using X-ray photoelectron spectroscopy (XPS). The specific surface area, pore diameter, and pore volume were determined using the Brunauer–Emmett–Teller (BET) method. The amount of dye loading and the light absorbance of the photoanodes were determined using UV–visible spectroscopy (UV–vis). To determine the dye loading, the dye was desorbed using NaOH solution (0.1 M). Cell performances were evaluated using a solar simulator (100 mW cm^{-2}, the equivalent of one sun at AM1.5G). The incident photon-to-electron conversion efficiency (IPCE) of the cells was determined. The electron transport was also investigated using intensity-modulated photocurrent/photovoltage spectroscopy (IMPS/IMVS) under light intensity of 15 mW cm^{-2} at wavelength of 455 nm.

3. Results and discussion

Mesoporous TiO_2 beads having various characteristics were obtained under most of the synthesis conditions, as shown in Table 1. Sample E was found to be nanoparticles (NPs) but not beads, as shown in Fig. 1A. In contrast to the P25 powders, the beads all exhibit pure anatase phase. The photoanodes made out of the obtained beads and NPs therefore exhibit pure anatase. The obtained beads vary in the size, ranging from 250 to 750 nm. Each bead consists of many nanoparticles, as shown in Fig. 1A, and each of the nanoparticles is a single crystal grain, as shown in Fig. 1B where the lattice spacing between the {1 0 1} planes, 0.35 nm, is also shown. The grain sizes, determined using the XRD spectra, vary as shown in Table 1. Comparison among the BET surfaces areas shows that all the beads have larger values than that of P25 powders. Among the beads, the specific surface area decreases with the grain size. Furthermore, the obtained beads have larger pore volumes, favoring more dye loadings. As shown in Table 1, the obtained beads exhibit different surface oxidation states. This was determined using XPS analysis (Fig. 2). Fig. 2A shows a high resolution spectrum of Ti2p for Sample D. Four peaks are seen after deconvolution and assigned to $Ti^{4+}2p_{3/2}$, $Ti^{3+}2p_{3/2}$, $Ti^{4+}2p_{1/2}$, and $Ti^{3+}2p_{1/2}$, located at 458.6, 457.9, 464.3, and 463.6 eV, respectively [18]. From the Ti2p spectra, the concentrations of Ti^{4+} were obtained and are given in Table 1. Table 1 shows that the higher hydrothermal temperature, the higher the Ti^{4+} concentration is, matching the trend of improved crystallinity with the hydrothermal temperature. In other words, a higher hydrothermal temperature leads to a lower oxygen vacancy concentration. All the beads show much higher Ti^{4+} concentrations than that of the P25 powders. Most of the beads have Ti^{4+} concentrations greater than 91%. Fig. 2B shows a high-resolution spectrum of O1s for Sample D. It is seen again that Ti_2O_3 is nearly absent, representing the fine surface of beads.

Using the samples shown in Table 1, six different types of photoanodes, having thicknesses in the range of 7.5–8.0 μm (Table 2), were made and evaluated for the light absorbance (Fig. 3A) and dye loading (Table 2). The light-harvesting efficiency (LHE) was then calculated from light absorbance by LHE = $1-10^{-la}$, where la is the light absorbance, and is also shown in Table 2. Photoanode VI composed of NPs exhibits better light absorbance or LHE than Photoanode I (P25-only). This is due to the dye loading of Photoanode VI is more than two times that of Photoanode I, as shown in Table 2. In fact, the all the hydrothermally synthesized

Table 2
Constituent, thickness, LHE, and dye loading of various photoanodes.

Photoanode ID	Sample ID	Thickness (μm)	Dye loading ($\times 10^{-7}$ mol cm^{-2})	LHE (%)
I	P25	8.0	2.37	58
II	A	7.5	6.12	70
III	B	7.8	5.48	65
IV	C	7.6	5.28	73
V	D	7.8	5.12	67
VI	E	7.8	4.96	62

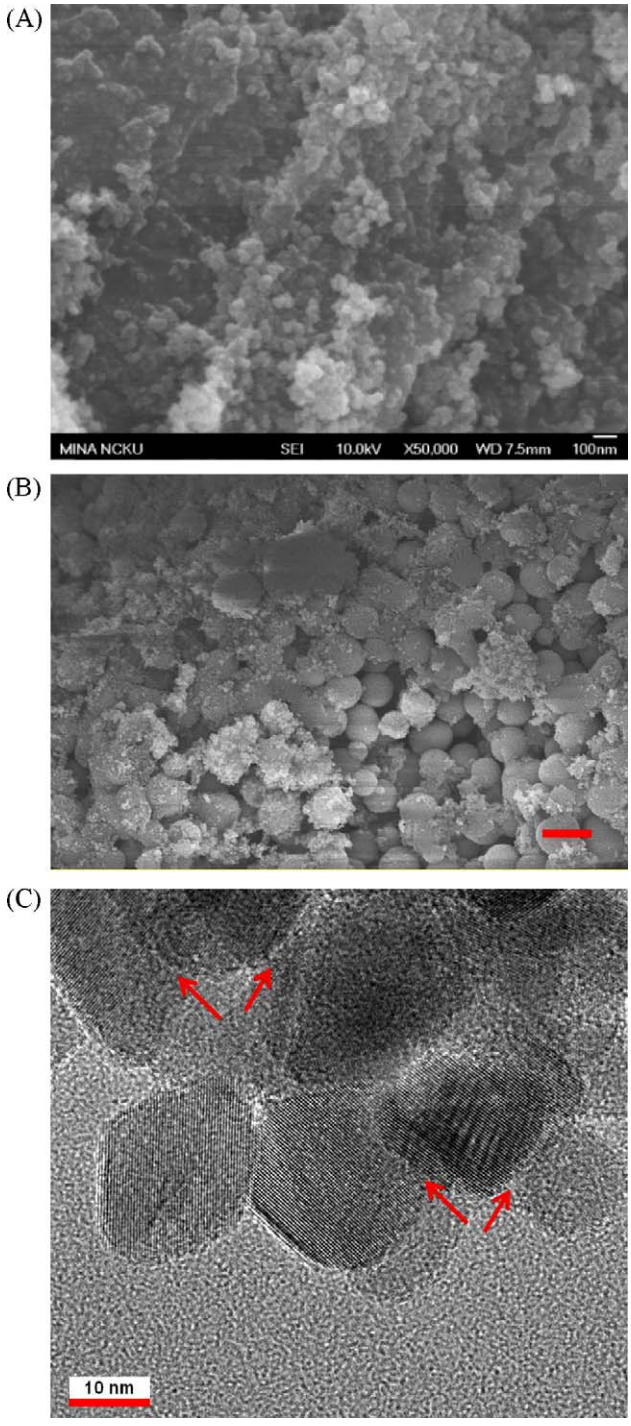

Fig. 1. SEM images of Samples (A) E and (B) B in Table 1. The scale bar in (B) is 1 μm. (C) HRTEM image of nanoparticles in TiO_2 beads (Sample D in Table 1). The interplanar distance is 0.35 nm, corresponding to anatase {1 0 1} planes. The arrows indicate the location of oriented attachment. The scale bar is 10 nm.

powders exhibit much better dye loadings than P25 powders. This is attributed to the higher specific surface areas and much larger pore volumes of the hydrothermally synthesized powders. However, the dye loading is not the major factor that determines the LHE when considering the photoanodes made out of the hydrothermally synthesized powders. Photoanodes II to VI, all consisting of pure hydrothermally synthesized powders, exhibit different LHEs and dye loadings, and the values of both are not in proportion. It was found that no correlation can be found between the LHE and the dye loading for the hydrothermally synthesized powders. On the other hand, LHE was found to vary with both the bead size and "bead size × dye loading" in very similar fashions as shown in Fig. 3B. The LHE increases with both the bead size and "bead size × dye loading" except that of Photoanode III, i.e., the one having the 750-nm beads. This clearly shows that the dominant factor is the bead size. In other words, the beads exhibit size-dependent Mie scattering. Photoanode III contains beads having the largest average size of 750 nm. We believe that severe light scattering occurs due to its largest average size. Therefore some of the incident light is reflected before having

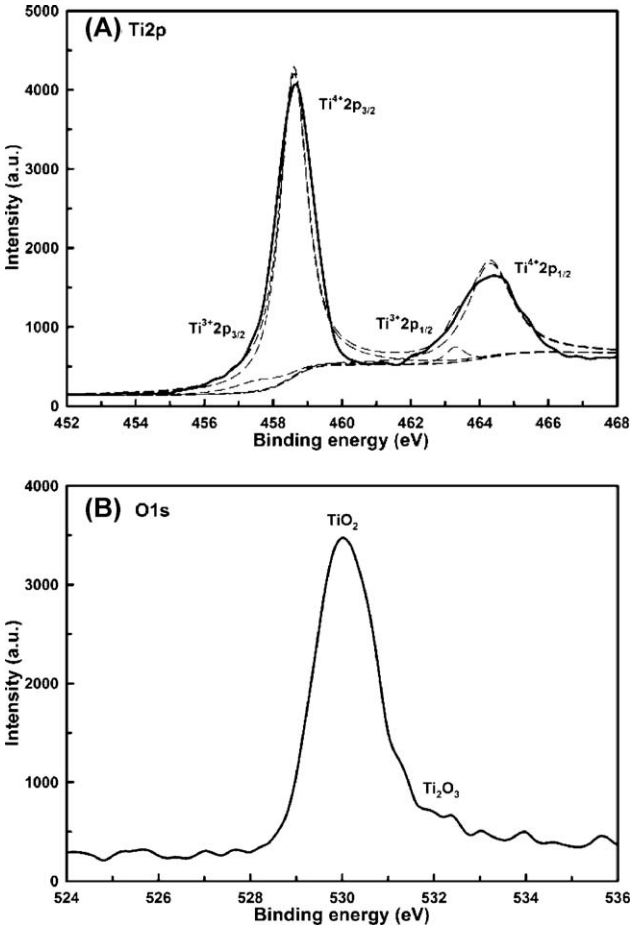

Fig. 2. XPS spectra of Sample D in Table 1. High resolution spectra of (A) Ti2p and (B) O1s.

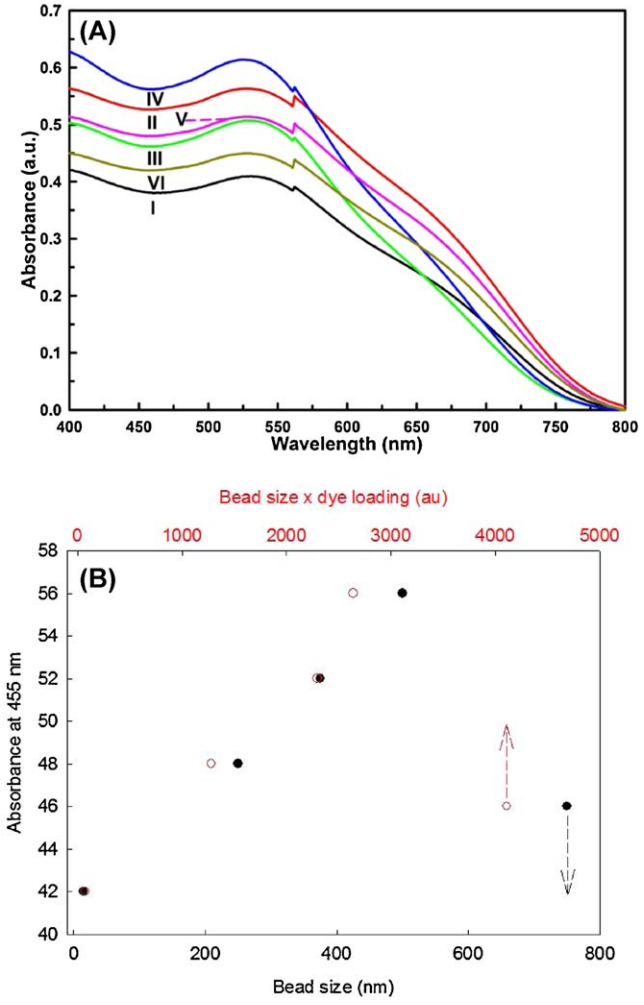

Fig. 3. (A) UV–visible light absorbance spectra of various N719-sensitized photoanodes. (B) Absorbance at 455 nm vs. bead size and "bead size × dye loading".

a chance to travel deeper into the photoanode and resulting in a lower LHE. Cells were fabricated using the resulting photoanodes and evaluated for the *J*–*V* behaviors.

Fig. 4 shows the *J*–*V* curves of these FDSCs. The values of short-circuit current (J_{sc}), open-circuit voltage (V_{oc}), fill-factor (FF), and efficiency (η) obtained from Fig. 4 are summarized in Table 3. Cell

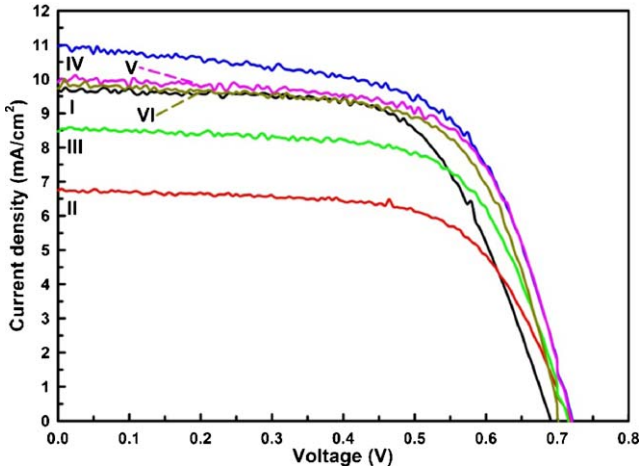

Fig. 4. The *J*–*V* curves of various FDSCs.

Table 3
J_{sc}, V_{oc}, FF, and η obtained from Fig. 4.

Cell ID	Sample ID	J_{sc} (mA cm^{-2})	V_{oc} (V)	FF (%)	η (%)
I	P25	9.69	0.69	64.1	4.29
II	A	6.72	0.72	65.1	3.16
III	B	8.47	0.71	66.6	4.03
IV	C	10.57	0.72	64.3	4.92
V	D	9.91	0.72	66.6	4.74
VI	E	9.73	0.71	66.6	4.56

I is a P25-only cell and have an efficiency of 4.29%. Cells II–V are bead-only cells and have different efficiencies varying from 3.16 to 4.92%. Cell VI is a hydrothermally synthesized NP-only cell and have an efficiency of 4.56%. As shown in Table 3, the efficiency is basically determined by the J_{sc}. It increases with J_{sc} quite linearly and does not correlate to V_{oc} or FF. The highest efficiency among these cells is Cell IV and its value reaches almost 5% which is 15% higher than that of Cell I, the P25-only cell. It is also seen that all the cells containing hydrothermally synthesized powders have higher FF and V_{oc} than the P25-only cell, except that the FF values of P25 and Sample C are similar. The higher FF represents less resistance. This is due to the pure anatase phase of the hydrothermally synthesized powders. The higher V_{oc} represents a higher electron density n in the conduction band of TiO_2 [19]. This is attributed to the higher dye loading and more light scattering. Further analyses using IMPS/VS and IPCE were conducted to evaluate the cell performance. The electron diffusion time τ_d obtained from IMPS analysis is shown in Table 4. Extremely fast diffusion times were obtained. The electron diffusion rates in photoanodes containing hydrothermally synthesized powders are 1–2 orders of magnitude faster than that of P25-only photoanode. This enhancement is attributed to the pure anatase phase and the existence of oriented attachment (Fig. 1B). The rutile-containing P25 powders lower the electron transport rate [20]. The oriented attachments which eliminate the large particle-to-particle interface resistance greatly enhance the electron transport. Correlations indicate that, among Cells II–VI, the value of τ_d generally decreases with the crystallinity and the Ti^{4+} concentration. Both better crystallinity and a high Ti^{4+} concentration favor faster electron transport. Among Cells IV–VI, which have the same crystallinity and surface oxygen vacancy concentration, the value of τ_d deceases with LHE and J_{sc}. Since the photoanodes have similar thicknesses, a higher LHE or larger J_{sc} indicates a higher n. More trap states would then be occupied due to the larger amount of electrons, leading to a trap-free diffusion for electrons [21]. Thus, the faster electron diffusion rates are obtained.

The electron lifetime τ_n obtained from IMVS analysis are also shown in Table 4. The τ_n of photoanodes containing hydrothermally synthesized powders are substantially lower than that of P25-only photoanode. The result is most possibly due to the difference in n. In general, the recombination rate is proportional to n^2, thereby a larger electron density would lead to a shorter τ_n [22–24]. Moreover, τ_n is usually be proportional to τ_d, as it has been reported that faster electron diffusion would have a larger possibility to encounter recombination species [25]. Among Cells II–VI,

Table 4
The values of electron diffusion time τ_d, electron lifetime τ_n, charge-collection efficiency η_{cc}, electron injection efficiency η_{inj}, and IPCE values at wavelength 455 nm.

Cell ID	τ_d (ms)	τ_n (ms)	η_{cc} (%)	IPCE (%)	η_{inj} (%)
I	12.40	65.1	81.0	24.5	51.9
II	1.30	2.9	55.2	19.0	49.3
III	0.53	4.7	88.7	24.0	41.4
IV	0.37	3.7	90.0	32.0	49.0
V	0.42	4.2	90.0	30.0	49.8
VI	0.47	4.2	88.8	29.5	53.6

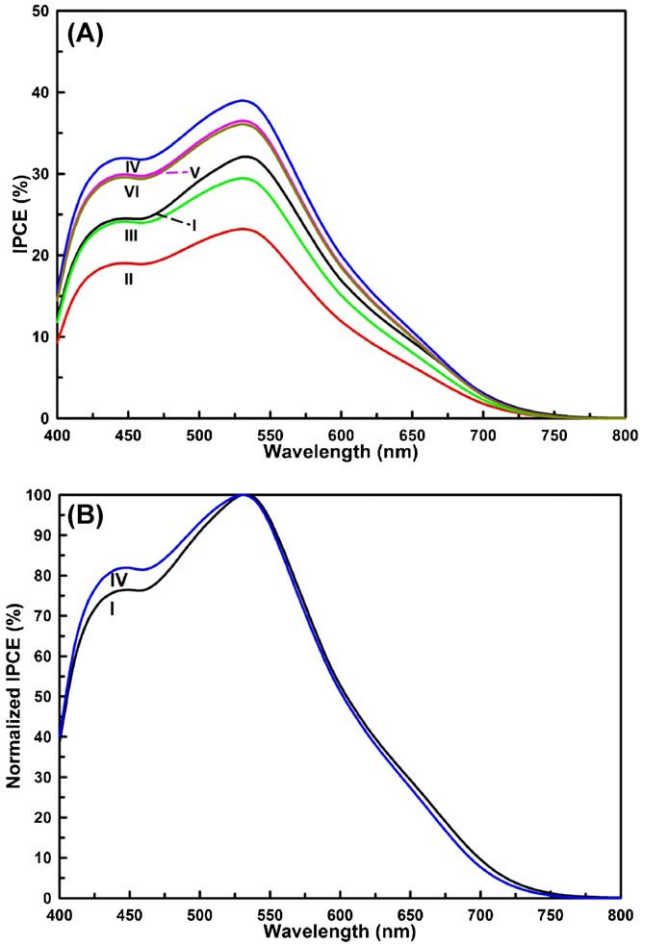

Fig. 5. (A) The IPCE curves of various FDSCs. (B) The normalized IPCE curves of selected FDSCs.

except Cell III, the τ_n tends to increase with Ti^{4+} concentration or reduced surface oxygen vacancy concentration. The exception of Cell I might be due to its lower J_{sc}, meaning a lower n. Among Cells IV–VI, which have the same surface oxygen vacancy concentrations but different bead sizes, the values of τ_n echo that of J_{sc} since a J_{sc} higher means a larger n while the photoanode thicknesses are similar, corresponding to a higher recombination rate.

The charge-collection efficiency $\eta_{cc} = 1 - \tau_d/\tau_n$ was determined as shown in Table 4 [8]. Except Cell II, the η_{cc} of the photoanodes containing hydrothermally synthesized powders is better than that of Cell I, the P25-only cell. Cell II has the longest τ_d and shortest τ_n. The result indicates that the enhancement of η_{cc} comes from the ultra-fast electron diffusion. The value would have been higher if the lifetime was longer. Fig. 5A shows the IPCE curves of various FDSCs and the IPCE values at 455 nm are shown in Table 4. The trend of IPCE curves under short-circuit condition matches that of J_{sc}. The electron-injection efficiency η_{inj} obtained using IPCE = LHE × η_{inj} × η_{cc} are summarized in Table 4. The η_{inj} of photoanodes containing hydrothermally synthesized powders are in general not much different from that of P25-only photoanode. The photoanodes in Cells I and VI both contain nanoparticles and have similar η_{inj}, representing that surface nature do not affect so much on η_{inj}. Among, Cells II–IV, we found that the η_{inj} strongly depends on the bead size, i.e., the η_{inj} decreases with the bead size. As the bead size increases, the inter-bead spaces also increases. Thus, a higher portion of the absorbed dye molecular accumulates in such spaces and thereby contributes no charge injection, resulting in lower η_{inj}. However, due to the ultra-fast electron diffusion and excellent light-harvesting ability, the resulting cells still exhibit enhanced efficiencies. Fig. 5B shows the normalized IPCE curves of Cells I and IV. The purpose of normalization is to eliminate the contribution from dye loading difference. The major enhancement due to the use of 500-nm-sized beads is in the range of 400–500 nm, indicating the stronger Mie scattering.

4. Conclusions

Mesoporous TiO_2 beads have shown their excellent advantages for use in RDSCs, in which the bead-containing photoanodes were prepared at elevated temperatures around 450 °C. In this study, we have demonstrated the first use of such mesoporous anatase TiO_2 beads with various sizes (250–750 nm) and characteristics in plastic substrate FDSCs, in which the photoanodes were prepared at room temperature. Due to the room temperature preparation, the use of mesoporous TiO_2 beads is not straightforward owing to the additive or binder burn-off issue. As a result, the concept of chemical sintering, which eliminates the step of additive removal, has been used to prepare bead-containing paste for the fabrication of photoanodes having good adhesion to the substrate. Also, a more efficient way, involving the use of hexamine severed as the steric agent, for the synthesis of the beads is demonstrated. Various plastic substrate FDSCs containing commercial P25 powders and the obtained beads were fabricated and evaluated. The pure anatase TiO_2 beads, having much lower oxygen vacancy concentrations than P25 powders and oriented-attachment grains greatly enhance the electron transport in the photoanodes. The large amount of electrons generated are attributed to the high dye loading and size-dependent Mie scattering of the beads. Increasing bead size leads to enhancing LHE due to Mie scattering except the 750 nm beads that gives too much scattering than desired. Nevertheless, we have demonstrated for the first time that the bead-only plastic substrate FDSCs not only can have efficiency as high as ~5% but also exhibit ultra-fast electron diffusion rates, less than 1 ms. The efficiency and electron diffusion rate are respectively 15% higher and two-order of magnitude faster than the P25-only cell.

Acknowledgment

This research was supported by the National Science Council in Taiwan under Grant No. NSC 99-2622-E-006-010-CC2.

References

[1] H. Lindstrom, A. Holmberg, E. Magnusson, S.E. Lindquist, L. Malmqvist, A. Hagfeldt, Nano Lett. 1 (2001) 97–100.
[2] M. Durr, A. Schmid, M. Obermaier, S. Rosselli, A. Yasuda, G. Nelles, Nat. Mater. 4 (2005) 607–611.
[3] N.G. Park, K.M. Kim, M.G. Kang, K.S. Ryu, S.H. Chang, Y.J. Shin, Adv. Mater. 17 (2005) 2349–2353.
[4] T. Yamaguchi, N. Tobe, D. Matsumoto, H. Arakawa, Chem. Commun. (2007) 4767–4769.
[5] K. Zhu, E.A. Schiff, N.G. Park, J. van de Lagemaat, A.J. Frank, Appl. Phys. Lett. 80 (2002) 685–687.
[6] B.A. Gregg, Coord. Chem. Rev. 248 (2004) 1215–1224.
[7] K. Zhu, N.R. Neale, A. Miedaner, A.J. Frank, Nano Lett. 7 (2007) 69–74.
[8] J. van de Lagemaat, N.G. Park, A.J. Frank, J. Phys. Chem. B 104 (2000) 2044–2052.
[9] K.D. Benkstein, N. Kopidakis, J. van de Lagemaat, A.J. Frank, J. Phys. Chem. B 107 (2003) 7759–7767.
[10] D.H. Chen, F.Z. Huang, Y.B. Cheng, R.A. Caruso, Adv. Mater. 21 (2009) 2206–2210.
[11] Y.J. Kim, M.H. Lee, H.J. Kim, G. Lim, Y.S. Choi, N.G. Park, K. Kim, W.I. Lee, Adv. Mater. 21 (2009) 3668–3673.
[12] W.G. Yang, F.R. Wan, Q.W. Chen, J.J. Li, D.S. Xu, J. Mater. Chem. 20 (2010) 2870–2876.
[13] S.R. Gajjela, K. Ananthanarayanan, C. Yap, M. Gratzel, P. Balaya, Energy Environ. Sci. 3 (2010) 838–845.
[14] F.Z. Huang, D.H. Chen, X.L. Zhang, R.A. Caruso, Y.B. Cheng, Adv. Funct. Mater. 20 (2010) 1301–1305.
[15] M.K. Nazeeruddin, A. Kay, I. Rodicio, R. Humphrybaker, E. Muller, P. Liska, N. Vlachopoulos, M. Gratzel, J. Am. Chem. Soc. 115 (1993) 6382–6390.

[16] H.C. Weerasinghe, G.V. Franks, J.D. Plessis, G.P. Simon, Y.B. Cheng, J. Mater. Chem. 20 (2010) 9954–9961.
[17] S. Eiden-Assmann, J. Widoniak, G. Maret, Chem. Mater. 16 (2004) 6–11.
[18] J.G. Yu, X.J. Zhao, Q.N. Zhao, Mater. Chem. Phys. 69 (2001) 25–29.
[19] P. Salvador, M.G. Hidalgo, A. Zaban, J. Bisquert, J. Phys. Chem. B 109 (2005) 15915–15926.
[20] N.G. Park, J. van de Lagemaat, A.J. Frank, J. Phys. Chem. B 104 (2000) 8989–8994.
[21] P.T. Hsiao, Y.L. Tung, H.S. Teng, J. Phys. Chem. C 114 (2010) 6762–6769.
[22] N.W. Duffy, L.M. Peter, R.M.G. Rajapakse, K.G.U. Wijayantha, J. Phys. Chem. B 104 (2000) 8916–8919.
[23] A.C. Fisher, L.M. Peter, E.A. Ponomarev, A.B. Walker, K.G.U. Wijayantha, J. Phys. Chem. B 104 (2000) 949–958.
[24] N. Kopidakis, K.D. Benkstein, J. van de Lagemaat, A.J. Frank, J. Phys. Chem. B 107 (2003) 11307–11315.
[25] A.J. Frank, N. Kopidakis, J. van de Lagemaat, Coord. Chem. Rev. 248 (2004) 1165–1179.